Experimental Shock-Wave Interference Heating on a Cylinder at Mach 6 and 8

Allan R. Wieting*
NASA Langley Research Center, Hampton, Virginia
and
Michael S. Holden†
Calspan-University of Buffalo Research Center, Buffalo, New York

This paper presents the details of an experimental study of shock-wave interference heating on a cylindrical leading edge representative of the cowl of a rectangular hypersonic engine inlet. The study, which was conducted at Mach numbers of 6.3, 6.5, and 8.0, has provided 1) detailed pressure and heat-transfer-rate distributions for a two-dimensional shock-wave interference on a cylinder and 2) insight into the effects of temperature-dependent specific heats on the phenomena. The peak pressure and heat-transfer rates were 2–25 times the undisturbed flow stagnation-point levels. The peak levels and their gradients increased with Mach number. Variation in specific heats and, hence, in the ratio of specific heats with temperature is manifested in slightly lower loads and amplification factors than for corresponding perfect-gas conditions.

Nomenclature

M = Mach number
p = pressure
q = heat-transfer rate
r = cylinder radius, 3.8 cm (1.5 in.)
Re = unit Reynolds number, 1/m (1/ft)
T = temperature, K (°R)
w = jet width
δ = shock generator or flow deflection angle
θ = angular position on cylinder, positive above undisturbed flow stagnation point

Subscripts

D = cylinder diameter
0 = undisturbed stagnation point value
p = peak value
T = total condition
∞ = freestream

Introduction

SHOCK-WAVE interference heating[1-4] is a critical problem in the structural design of the thermal protection system and the load-carrying structure of high-speed vehicles such as the Orient Express and Shuttle II. Extremely high-pressure and heat-transfer-rate gradients can occur in highly localized regions where the interference pattern impinges on the surface. The extreme heat-transfer rate and gradients that occur over this narrow impingement region result in large temperature gradients and their attendant thermal stresses,[5] which limit the useful life of the structural component. The peak pressure and heat-transfer rates and distributions are sensitive to Mach number, freestream flow conditions, and shock strength.[1-4,6]

Experimental studies to date on these phenomena have focused primarily on planar shocks intersecting shock systems generated by three-dimensional bodies or cylinders oriented transverse to the oblique shock (i.e., representative of a wing or tail).[1-4] This left a void for the designer of two-dimensional engine inlets, which would have planar shocks from the inlet compression surfaces intersecting a cylindrical leading edge oriented with its axis parallel to the plane of the shock. In 1971, Craig and Ortwerth[7] experimentally measured pressures and heat-transfer rates on a cylindrical leading edge typical of a hypersonic inlet cowl. However, large instrumentation spacing resulted in poor resolution of the peak pressure and heat-transfer rates.

Several investigators have attempted analytical solutions of the shock flowfield. Edney[4] and Morris and Keyes[8] used oblique shock and Prandtl-Meyer expansion relationships to predict the interference pattern and peak pressure and heat-transfer rate, with good success. However, their methods rely on experimental measurements of the shock stand-off distance and transmitted shock length. Tannehill and Holst[9] applied a two-dimensional Navier-Stokes finite-difference analysis in a simulation of Edney's spherical leading-edge results, with some success. However, the central-difference formulation could not adequately capture the shocks at the high Reynolds numbers of the tests. Recent advances have proved more rigorous; see, for example, Refs. 10 and 11.

A unified set of experiments for a cylindrical leading edge oriented with its axis parallel to the plane of the impinging shock is needed for the design of cowl leading edges for rectangular hypersonic engine inlets. This paper presents the experimental results from tests in the NASA Langley Research Center 8-ft High-Temperature Tunnel (8-ft HTT) at a Mach number of 6.5 and the Calspan 48-in. Hypersonic Shock Tunnel (48-in. HST) at Mach numbers of 6.3 and 8.0. The model consisted of a 7.6-cm- (3-in.) diam cylinder and a shock generator wedge articulated to angles of 10, 12.5, and 15 deg. Stream Reynolds numbers ranged from 1.6×10^6 to 16×10^6/m (0.5×10^6 to 4.9×10^6/ft), and total temperature ranged from 1200 to 1900 K (2100 to 3400°R). Model position was varied to obtain type III, type IV, and type V interference patterns, as defined by Edney.[4] The majority of the results are for the type IV interference pattern because it results in the most severe pressures and heat-transfer rates. Complete details of the study can be found in Ref. 6.

Shock-Wave Interference Patterns

The first step in determining the effects of shock impingement on the pressure and heat-transfer rate is to determine the

Presented as Paper 87-1511 at the AIAA 22nd Thermophysics Conference, Honolulu, HI, June 8-10, 1987; received July 13, 1987; revision received Oct. 14, 1988.

*Head, Aerothermal Loads Branch. Member AIAA.
†Principal Scientist. Member AIAA.

interference pattern that will exist when two oblique shocks of different strengths intersect. The type of interference pattern obtained is dependent on the relative strengths of the intersecting shocks and the geometry of the body on which the extraneous shock will impinge. Edney[4] defined six types of shock-wave interference patterns, all of which can occur when an oblique shock intersects the bow shock of a leading edge. The six patterns are shown in Fig. 1, which also shows how the interference patterns change as the impinging shock/bow-shock intersection point moves circumferentially around the cylinder. The leading-edge schematic in the center of the figure shows the approximate angular regions and the interference type that will result when the oblique shock intersects the bow shock in that region. Each of the six interference patterns or types are shown around the left periphery of the figure. Three of the interference patterns (I, II, and V) result in shock/boundary-layer interactions. Type III results in an attaching shear layer, and type VI results in an expansion-fan/boundary-layer interaction. Type IV is characterized by an impinging or grazing supersonic jet. The type III and IV interference patterns were the subject of this investigation. The details of the interference patterns are given quite eloquently by Edney,[4] and the reader is urged to read his work. The interference patterns that occur in this study (III, IV, and V) will be briefly described next.

Type III Interference

A type III interference pattern occurs when a weak shock intersects a strong shock (flow behind shock is subsonic) as shown in Fig. 1. The flow in the region above the shear layer is subsonic, and the flow between the shear layer and transmitted shock is supersonic. Depending on the angle the shear layer makes with the tangent to the body surface, the shear layer will be undeflected and attached to the surface. The supersonic flow is deflected downward through an oblique shock, the strength of which depends on the Mach number and flow turning angle. Pressure and heat-transfer-rate amplification caused by the attaching shear layer is analogous to a reattaching separated boundary layer. The heat-transfer rate is dependent on the Reynolds number of the impinging flow, based on the shear-layer length. The state of the shear layer (laminar or turbulent) is a critical parameter in determining the pressure and heat-transfer rates.

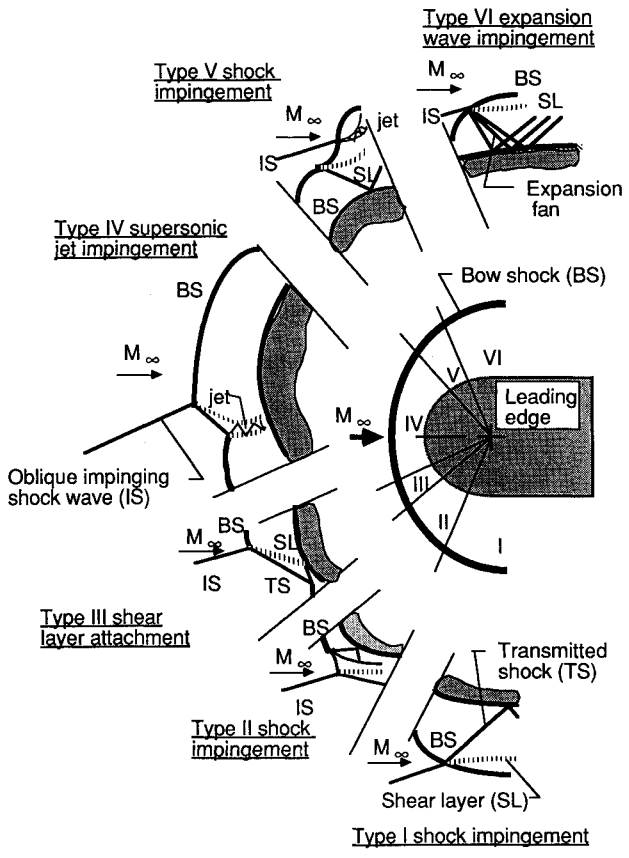

Fig. 1 Six types of shock-wave interference patterns.

Type IV Interference

The type IV supersonic jet interference pattern occurs when an oblique shock wave intersects the nearly normal part of the bow shock from a blunt leading edge. The intersection results in further displacement of the bow shock and the formation of a supersonic jet contained between two shear layers and submerged within the subsonic shock layer between the body and the bow shock wave. A jet bow shock is produced when the jet impinges on the surface, creating a small region of stagnation heating. The maximum pressure and heat-transfer rate occur when the jet impinges perpendicular to the surface.

Type V Interference

A type V interference pattern occurs when the impinging shock intersects the bow shock just above the upper sonic line, as shown in Fig. 1. This pattern is analogous to the type II interaction, except that a supersonic jet instead of a simple shear layer is formed at the point of intersection. The jet is much thinner then the type IV jet and is generally indistinguishable from a shear layer. The shear layer and the jet converge downstream and diffuse without impinging on the leading edge. However, a shock wave is formed just below the intersection point and results in a shock-wave/boundary-layer interaction on the leading edge.

Facilities

The NASA Langley Research Center 8-ft High-Temperature Tunnel (8-ft HTT) is a hypersonic blowdown tunnel in which the high energy level for simulating hypersonic flight is obtained by burning methane and air in a high-pressure combustor. The resulting combustion gases are expanded through a conical, contoured, 2.4-m (8-ft) exit diameter nozzle to obtain a nominal Mach 7 flow in an enclosed 3.7-m (12-ft)-long open-jet test section. Downstream of the test section, flow enters a straight-tube supersonic diffuser and is pumped to the atmosphere by a single-stage annular ejector. The facility is capable of simulating true-temperature flight conditions for altitudes from 24 to 37 km (80 to 120 kft) for test times up to 120 s.

The 8-ft HTT is equipped with a hydraulically operated elevator to which the model to be tested is mounted. The 13.6-metric ton (15-ton) elevator can raise or lower the model 2.2 m (85 in.) into or out of the hot test stream in 1.5 s. During tunnel startup and shutdown, the model is held out of the test stream to avoid the severe loads associated with these transient flow conditions.

The Calspan 48-in. Hypersonic Shock Tunnel (48-in. HST) is started by rupturing a double diaphragm, which permits the high-pressure gas in the driver section to expand into the driven section and, in so doing, generates a normal shock that propagates through the low-pressure air. A region of high-temperature, high-pressure air is produced between this normal shock front and the gas interference between the driver and driven gas, often referred to as the contact surface. When the primary or incident shock strikes the end of the driven section, it is reflected, leaving a region of almost stationary high-pressure heated air. This air is then expanded through a contoured nozzle to the test section.

The duration of the flow in the test section is controlled by the interactions among the reflected shock, the interface, and the leading expansion wave generated by the nonstationary expansion process in the driver section. The initial conditions of the gases in the driver and driven sections are controlled so that the gas interface becomes transparent to the reflected shock, in order that no waves are generated by the interface

reflected shock interaction. This is known as a tailored interface condition. Under these conditions, the test time is controlled by the time taken for the driver-driven interface to reach the throat or the leading expansion wave to deplete the reservoir of pressure behind the reflected shock.

Models

The test models consisted of 321 stainless steel cylinders, 1.3 cm (0.50 in.) thick, 61 and 46 cm (24 and 18 in.) long, and 7.6 cm (3.0 in.) in diameter, and a sharp leading-edge shock generator, which could be articulated 10, 12.5, and 15 deg to the freestream flow. A photograph of the 46-cm-long model in the 48-in. HST test section is shown as Fig. 2. The shock generator and cylinder could be translated horizontally and vertically relative to each other to facilitate obtaining the desired shock intersection location; hence, the desired shock interaction. In addition, the cylinder could be rotated about its axis to place the high-density instrumentation in the interaction zone. The cylinder was mounted with its axis parallel to the plane of the shock generator.

Instrumentation

Instrumentation location was similar for both test series; however, the type of instrumentation differed because of the different exposure times or test times of the two facilities. Typically, the test time in the 8-ft. HTT was 5 s; hence, chromel-constantan and chromel-alumel coaxial thermocouples and low-frequency strain-gage types of pressure transducers were used. A few high-frequency transducers, which have to be mounted nearly flush with the surface, were used but failed because of the high-temperature exposure after a few runs. The test time in the 48-in. HST was 15 ms; hence, high-frequency pressure transducers and thin film platinum resistance thermometers mounted on a Pyrex substrate (see Fig. 2) were used. Limited pressure and heat-transfer rates were obtained on the shock generator. The 8-ft. HTT model had 46 pressure and thermocouple locations. Sixteen of these locations were 1 deg or 0.666 mm (0.0262 in.) apart, and the remainder were 3.33 mm (0.131 in.) apart. The Calspan model had 25 pressure locations and 50 heat-transfer locations. The pressure locations were 2.4 deg and 1.59 mm (0.0625 in.) apart. The heat-transfer gage spacing was 0.76 deg or 0.51 mm (0.020 in.) apart in the high-density area (19 gages) and 3.05 deg or 2.0 mm (0.080 in.) apart elsewhere.

Pressure, thermocouple, and thermometer gage output was converted to engineering units in the normal manner. The temperature histories were converted to heat-transfer rates using a numerical procedure based on the solution for a semi-infinite solid with temperature-dependent properties.[12] Overall accuracy was within 5%. More detail is given in Ref. 6; however, the data from the 48-in. HST reported in Ref. 6 were inadvertently not corrected for temperature-dependent properties. The corrected data are used herein and are available from the author.

Tests and Test Procedures

The tests in the 8-ft HTT were at a Mach number of 6.5, a total temperature of 1900 K (3400 R), and a freestream unit Reynolds number of 1.6×10^6/m (0.5×10^6/ft). The shock generator angle was fixed at 10 deg. The main variable in this test series was the cylinder height relative to the wedge. The height was varied 3.3 cm (1.3 in.) over 12 different positions to map the interference patterns over a wide range of shock intersection locations. Schlieren pictures of the flowfield were obtained at a rate of 20 frames/s, using an X75 Xenon lamp with a 0.38-mm (0.015-in.)-diam source and a 6-μs spark duration.

The tests in the Calspan 48-in. HST were at Mach numbers of 6.3 and 8.0, total temperatures ranging from 1200 to 1700 K (2100 to 3040 °R), and freestream unit Reynolds numbers of 2.4×10^6 to 16×10^6/m (0.72×10^6 to 4.9×10^6/ft). The purpose of this series was to determine the effect of shock strength, Reynolds number, and Mach number on the pressure and heat-transfer-rate distributions. Single-frame schlieren was obtained.

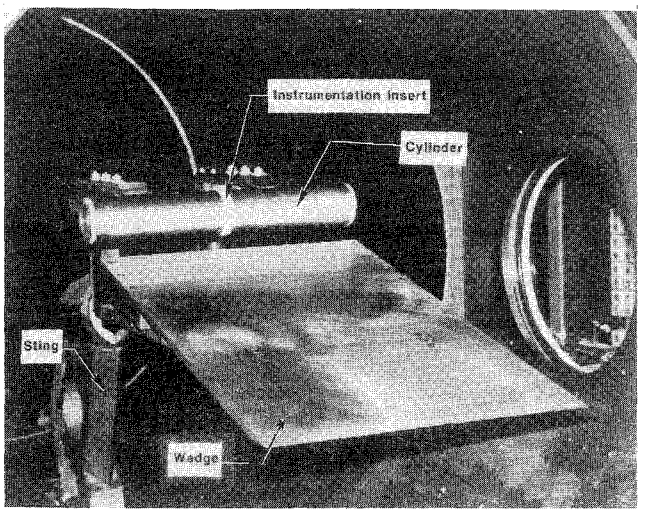

Fig. 2 Photograph of shock generator wedge and cylinder in the Calspan 48-in. HST.

Pressure and heat-transfer-rate distributions (herein referred to as undisturbed) were obtained on the cylinder at one Reynolds for each Mach number, with the shock generator removed to serve as a direct indication of the effect of the shock-wave interference on the pressure and heat-transfer-rate levels and distributions.

Results and Discussion

The undisturbed pressures and heat-transfer rates, normalized by the measured stagnation-point value, are plotted in Fig. 3 as a function of angular position (θ) measured in degrees from the horizontal centerline of the cylinder. Data are presented for the Mach 6.5 8-ft HTT tests and the Mach 6.3 and 8.0 48-in HST tests. The undisturbed baseline distributions compare very well with a viscous shock layer (VSL) solution at Mach 6.3.[6] However, the predicted stagnation pressure and heat-transfer rate were 2% and 18 to 50% lower than the experimental values, respectively. Similar results were obtained with the method of Fay and Riddell[13] modified for two-dimensional flow. The difference is attributed to freestream turbulence generated by the nozzle boundary layer, which is not accounted for in the analyses. Since the freestream turbulence is present for both the undisturbed and shock-interference tests, the data are normalized by the measured q_0 to attenuate the effect on the heat-transfer-rate amplification ratios. The VSL result is repeated in the other plots to help visualize the interference effects.

Several runs were duplicated to demonstrate the repeatability of the facilities test conditions and model data. Data repeatability was excellent; hence, the data at different flow conditions can be compared with confidence that any differences are due to flow variables and not to anomalous facility behavior.[6]

Spanwise pressure measurements on the wedge and cylinder were used to demonstrate uniformity or two-dimensionality of the flow over the cylinder with and without shock-interference flow. The data indicated that the flow was uniform 25.4 cm (10 in.) to either side of the center for undisturbed flow and 14 cm (5.5 in.) to either side for a type IV interference.[6]

A typical pressure and heat-transfer-rate distribution along the circumference of the cylinder for the type IV jet interaction is given in Fig. 4. Included for comparison are the undisturbed pressure and heat-transfer-rate distributions. The corresponding schlieren photographs are shown in Fig.5. The results shown are for Mach 8.03, a Reynolds number of 5.08×10^6/m (1.55×10^6/ft), and a shock generator angle of 12.5 deg. The peak pressure amplification (ratio of peak

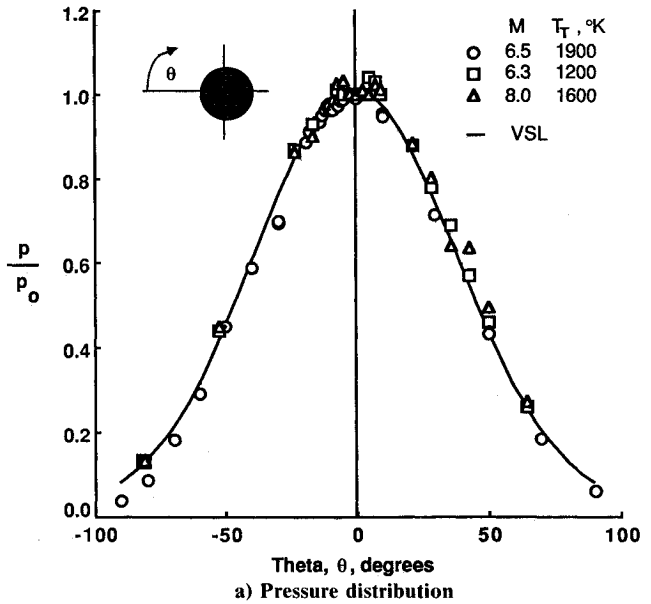

a) Pressure distribution

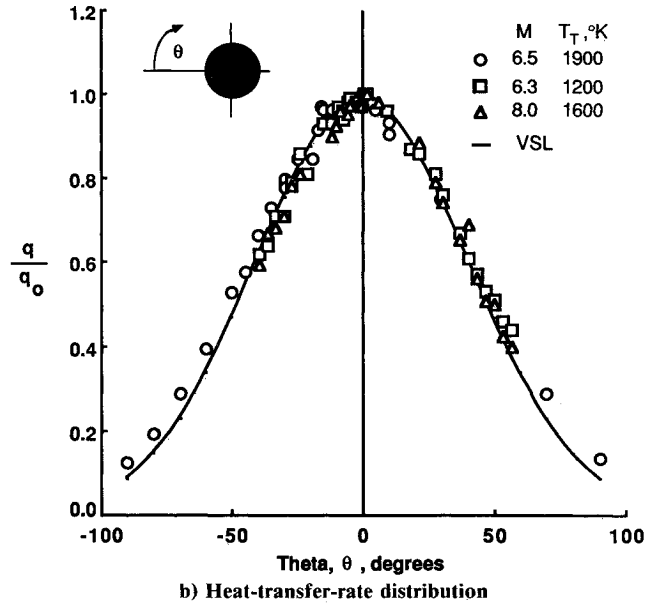

b) Heat-transfer-rate distribution

Fig. 3 Undisturbed pressure and heat-transfer-rate distributions.

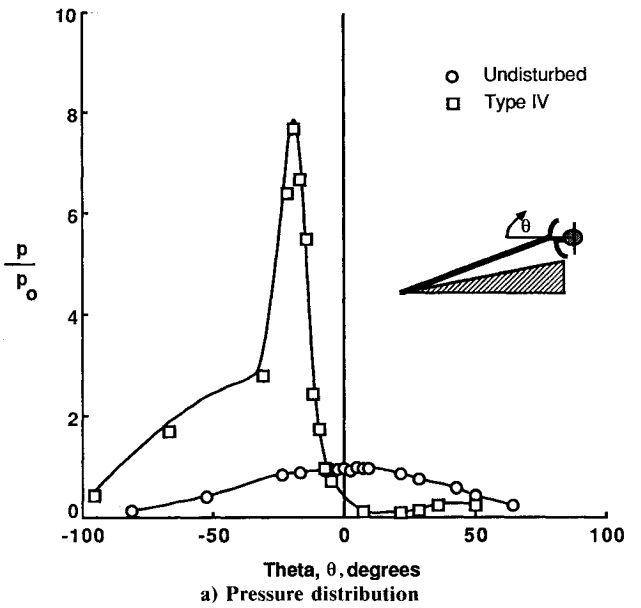

a) Pressure distribution

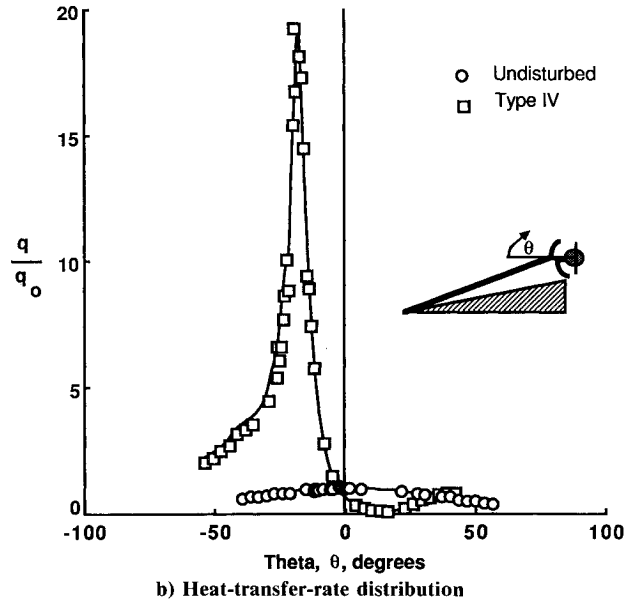

b) Heat-transfer-rate distribution

Fig. 4 Typical pressure and heat-transfer-rate distributions for a type IV interference pattern.

pressure or heat-transfer rate caused by the impingement of the shock-wave interference pattern to the undisturbed free-stream stagnation pressure or heat-transfer rate) is 7.67 and occurs at $\theta = -19.1$ deg. The peak heat-transfer-rate amplification is 19.25 (note that this value more than doubled when material property temperature dependency was taken into account) and occurs at $\theta = -19.6$ deg. Comparison of the schlieren photographs (Fig. 5) show that the intersection caused the bow-shock displacement to increase from 1.5 cm (0.58 in.) to 2.87 cm (1.13 in.).

Effect of Shock Intersection Point

The type of intersection pattern obtained depends on the strength of the impinging shock and the point of intersection on the body's bow shock, as shown in Fig. 1. The pressure and heat-transfer-rate amplifications depend on both the interference pattern and the flow angle of incidence with the surface. The cylinder was moved relative to the shock generator to change the intersection point of the shocks. The interference pattern and pressure and heat-transfer-rate distributions changed as shown in Figs. 6 and 7 for tests at Mach 6.5. The schlieren photographs indicate that types V (not conclusively), IV, and III interference patterns occurred. The corresponding pressure and heat-transfer-rate distributions differ significantly as shown in Fig. 7.

The sensitivity of the pressure and heat-transfer-rate amplification ratio to the impinging-shock bow-shock intersection point is best observed by plotting the peak amplification ratio for each run as a function of angular position of the peak, creating a locus of the peak amplification ratios. The key variable for changing the intersection point is the vertical height of the cylinder above the wedge trailing edge. The Mach 6.5 (8-ft HTT) and Mach 6.3 and 8.0 (48-in. HST) heat-transfer-rate data for a shock generator angle of 10 deg are compared in Fig. 8. Comparison of the amplification ratio at a given location with the undisturbed level at the same location yields an indication of the local range in pressure and heat-transfer rate, to which the cylinder is exposed.

The three sets of data show similar trends but different amplification levels. The Mach 6.5 data are used in the following discussion of the effect of the shock intersection point on the data trend. As the impinging shock wave moved downward from a maximum bow-shock intersection point of 2.2 cm (0.86 in.) above the centerline of the cylinder (Fig. 6a) to an intersecting point of 1.0 cm (0.41 in.) below the cylinder centerline (Fig. 6b), the heat-transfer-rate amplification increased

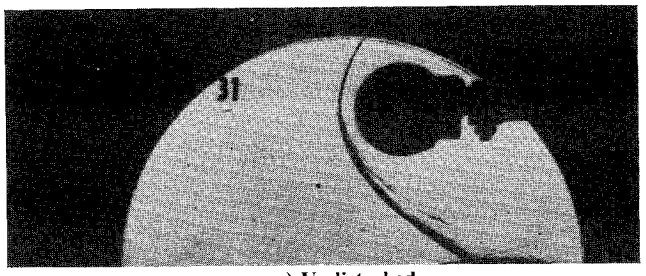

a) Undisturbed

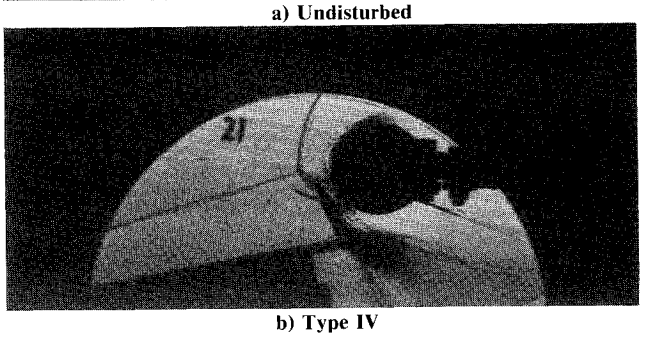

b) Type IV

Fig. 5 Schlieren photograph of undisturbed flow and type IV interference pattern.

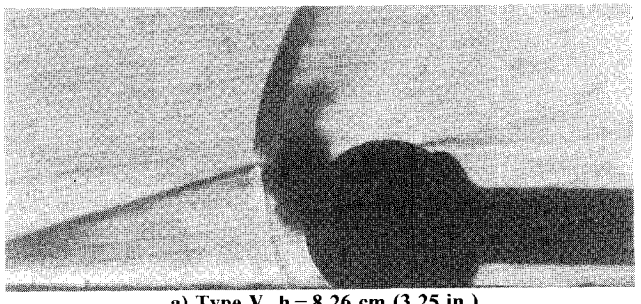

a) Type V, h = 8.26 cm (3.25 in.)

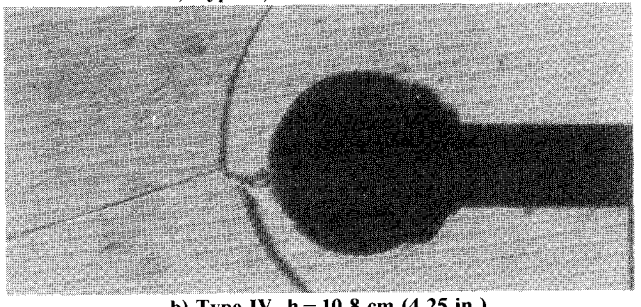

b) Type IV, h = 10.8 cm (4.25 in.)

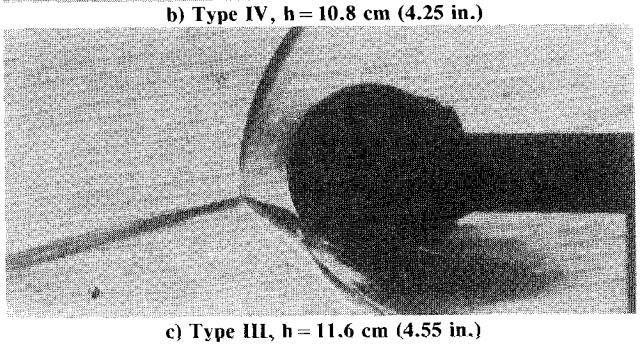

c) Type III, h = 11.6 cm (4.55 in.)

Fig. 6 Effect of shock intersection point on interference patterns.

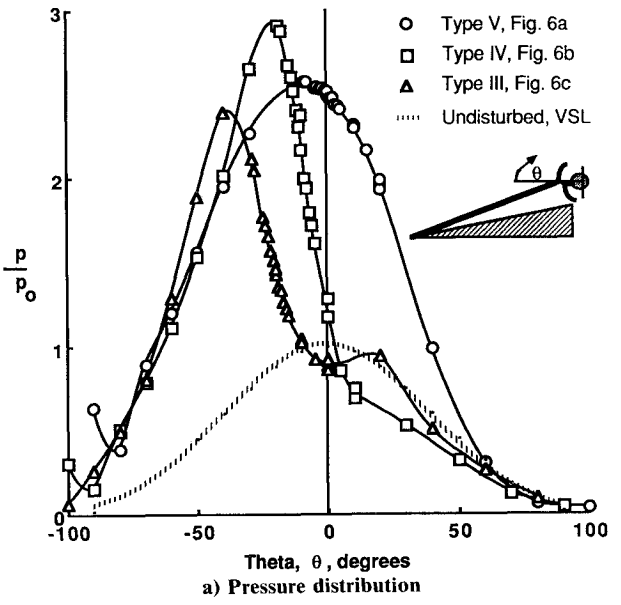

a) Pressure distribution

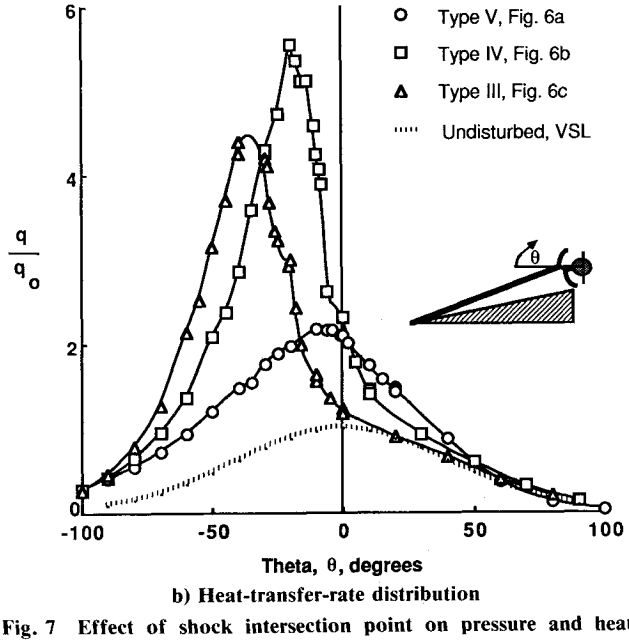

b) Heat-transfer-rate distribution

Fig. 7 Effect of shock intersection point on pressure and heat-transfer-rate distributions.

rapidly from 2.16 at $\theta = -4$ deg to the maximum of 5.58 at $\theta = -20$ deg. During this process, the shock-wave interference pattern changed from a type V to a type IV interference pattern in which the jet impinged nearly normal to the surface. Note that it is not clear from the schlieren photograph (Fig. 6a) that a type V interference pattern did occur.

As the impinging shock moved further downward to an intersection point 1.3 cm (0.50 in.) below the cylinder centerline, the heat-transfer-rate amplification decreased from the maximum to 4.20 at $\theta = -30$ deg (Fig. 6c). During this process, the interference pattern changed from a type IV to a type III interference pattern. The heat-transfer-rate amplification for a type III interference is a strong function of the shear-layer state. The shear-layer Reynolds number (based on the Mach 2.20 flow conditions below the shear layer and the measured shear-layer length of 3.35 cm (1.32 in.) for this run was 1.08×10^5, which is above the transition Reynolds number of 6×10^4 measured by Birch and Keyes.[14] Therefore, the shear layer is turbulent, and the heat-transfer-rate amplification should be near its maximum for a type III interference for these conditions.

As stated earlier, the 8-ft HTT data differ in level from the 48-in. HST data. For example, the maximum measured heat-transfer-rate amplification at Mach 6.3 (48-in.HST) was 11.65 and occurred at $\theta = -38.2$ deg. This corresponds to 5.58 at $\theta = -20$ deg for the Mach 6.5 8-ft HTT data. In both cases, the maximum heat-transfer-rate amplification occurred for a type IV interference pattern in which the jet impinged nearly normal to the surface. The data are at nearly the same Mach number but differ in both Reynolds number and stream total

temperature. As will be discussed later, the effect of Reynolds number is negligible since the shear-layer Reynolds number indicates that the shear-layer flow would be turbulent. The effect of Mach number over this small range is small, as can be seen by comparing the Mach 8 and 6.3 data from the 48-in. HST, which is shown in the figure. Consequently, as shown in Ref. 6, the differences between the Mach 6.5 and 6.3 data are due to the variation of the specific heats with temperature (variable specific heat ratio). These effects manifest in slightly smaller flow turning angles across shocks, which result in larger jet widths than the corresponding perfect-gas conditions. More important, the variation of the specific heat with temperature are shown to decrease the pressure and heat-transfer levels and amplification ratios, which are in contrast to the conclusions of Edney[4] and Keyes and Hains.[3]

Impinging Shock Strength

The peak pressure (p_p/p_0) and heat-transfer-rate (q_p/q_0) amplifications for Mach 8.0 are plotted as a function of their location θ for each wedge angle (10, 12.5, and 15 deg) in Figs. 9 and 10, respectively. The undisturbed distributions are also shown for comparison purposes. The maximum pressure amplification occurs at approximately $\theta = -20$ deg and the maximum heat-transfer-rate amplification at approximately $\theta = -22$ deg. Because of the different spacing for the pressure and heat-transfer measurements, it is difficult to determine if the peaks would occur at the same location. The data trend at each shock strength (wedge angle) shows the effect of shock intersection point as discussed in the previous section. Edney[3] and Keyes and Hains[4] reported similar trends for the various models tested.

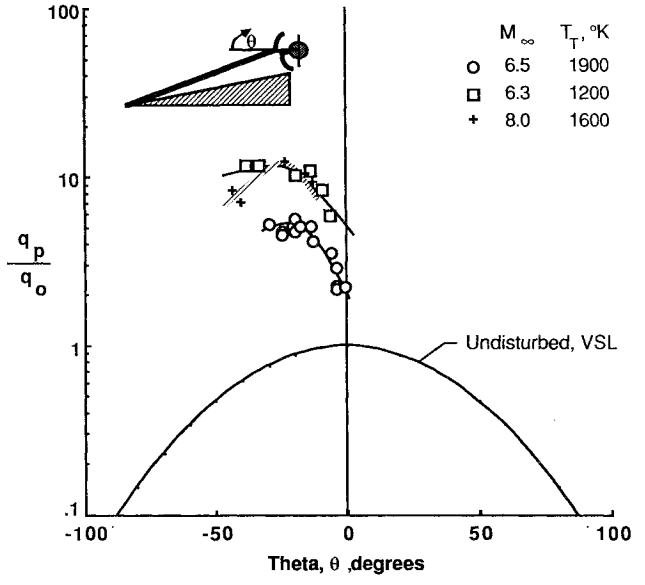

Fig. 8 Effect of shock intersection point on locus of peak heat-transfer-rate amplifications.

The peak pressure amplification (Fig. 9) at a given point on the cylinder increased with increasing impinging shock strength. The pressure amplification at $\theta = -20$ increased from 6.36 at $\delta = -10$ deg to 7.67 at $\delta = -12.5$ deg to 12.02 at $\delta = -15$ deg. The magnitude of the differences was due primarily to changes in the interference pattern, i.e., shock stand-off distance, transmitted shock length, jet width, and jet flow inclination relative to the cylinder surface.[6] Schlieren photographs of the interference patterns, which result in the maximum amplification ratios, are shown in Fig. 11. Schlieren measurements indicate that the shock standoff and transmitted shock length increased with flow deflection angle or shock strength but at different rates; and the transmitted shock-wave angle became shallower with increasing flow deflection angle. Because the effects of these parameters are interrelated, the perfect-gas code developed by Morris and Keyes[8] was used in Ref. 6 to substantiate the data trends. The results showed that 1) the peak pressure amplification would increase with shock strength to a maximum and then decrease with further increases in shock strength, 2) the jet flow angle increased from 15 to 32 deg, which can result in a significant difference in the actual pressure rise since the pressure rise depends on how much the jet flow is turned by the cylinder surface, and 3) the jet width also increased.

The heat-transfer-rate amplifications (Fig. 10) for a fixed wedge angle show similar trends to the pressure amplifications. However, for a given location on the cylinder the amplification increased as the wedge angle was increased from 10 to 12.5 deg, but the heat-transfer-rate amplification decreased when the wedge angle was increased to 15 deg. This trend reversal was a result of the jet width increasing as the deflection angle increased. Edney showed that the peak heat-transfer-rate amplification is proportional to the square root of the product of the ratio of body radius to jet width and the peak

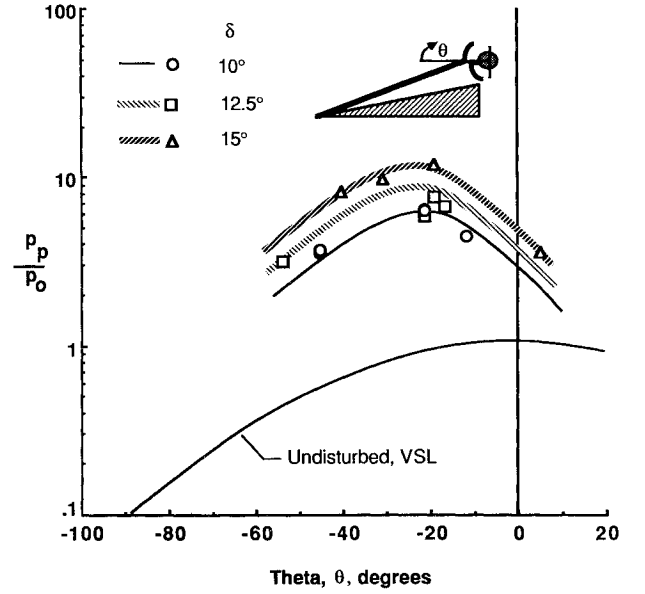

Fig. 9 Effect of impinging shock strength on the locus of peak pressure amplification, Mach 8.0.

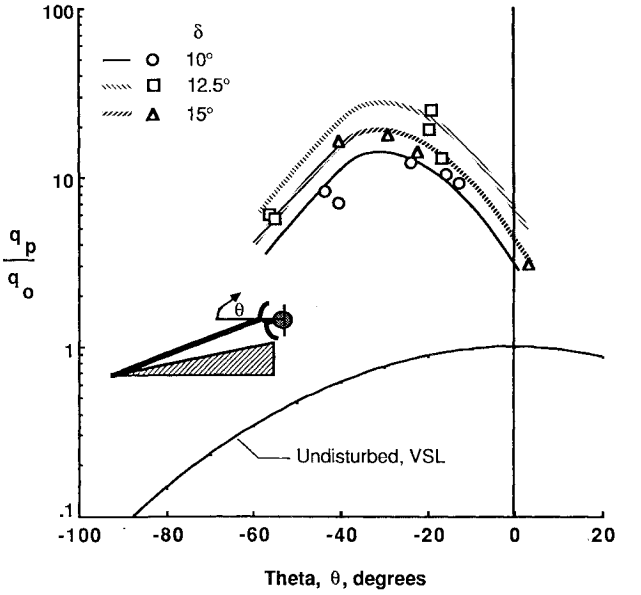

Fig. 10 Effect of impinging shock strength on the locus of peak heat-transfer-rate amplification, Mach 8.0.

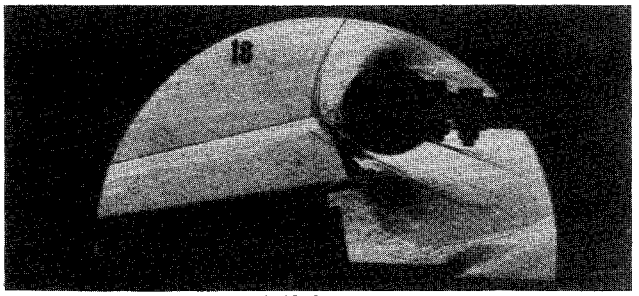

a) 10-deg wedge

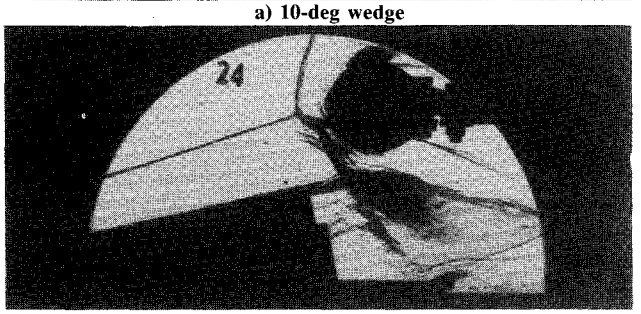

b) 12.5-deg wedge

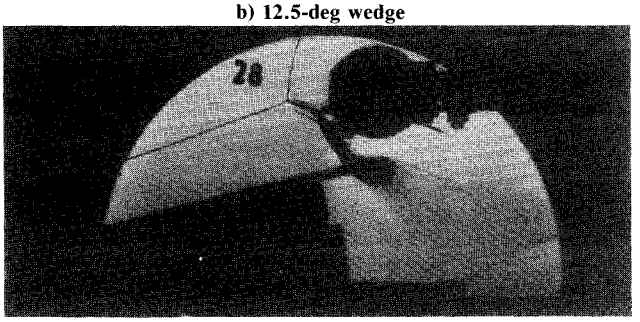

c) 15-deg wedge

Fig. 11 Effect of impinging shock strength on type IV interference patterns.

pressure amplification ratio. Because the jet width increased faster with shock strength than the pressure amplification ratio, the maximum heat-transfer-rate amplification occurred at a different shock strength than the maximum pressure amplification.

Effect of Unit Reynols Number

The effect of unit Reynolds number was investigated by changing the reservoir pressure or stream total pressure. The Mach 8 data obtained at Reynolds numbers of 2.5×10^6, 5.08×10^6, and 12.5×10^6/m (0.77×10^6, 1.55×10^6, and 3.80×10^6/ft) and a wedge angle of 12.5 deg are plotted in Fig. 12 as a function of angular position. The schlieren photographs, two of which are shown in Figs. 5b and 11b, indicate type IV interference patterns. The data show a definite effect of Reynolds number; however, under closer inspection, we see that Reynolds number is not the only variable in this data set. Although the cylinder and wedge position were fixed, the shock intersection point was slightly different for each Reynolds number. As the Reynolds number was changed, the wedge boundary-layer displacement thickness changed. Consequently, the shock wave was displaced different distances from the wedge, which resulted in the impinging shock intersecting the bow shock at different locations.

The sensitivity of the heat-transfer-rate amplification to the shock impingement point was shown in Figs. 8 and 10. The small displacements in the intersection point resulted in jet impingement points on the cylinder of -16.71, -19.58, and -19.08 deg. As a consequence, the heat-transfer-rate amplification increased from 12.99 to 25.05 as the Reynolds number increased. The pressure and heat-transfer-rate amplification trends of these three data sets agree with the trends observed when the shock-wave intersection point was changed as shown

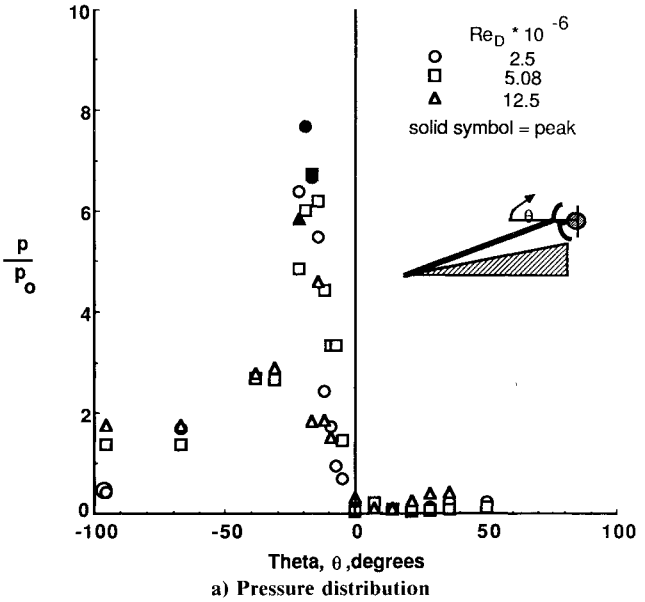

a) Pressure distribution

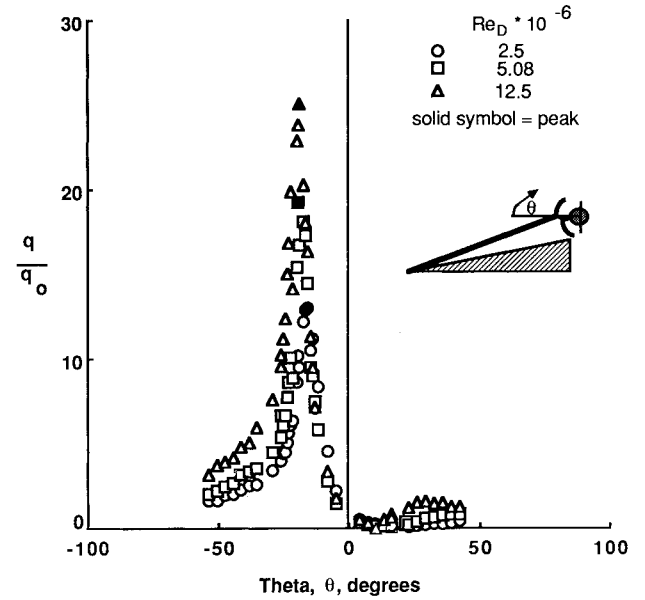

b) Heat-transfer-rate distribution

Fig. 12 Effect of freestream unit Reynolds number on pressure and heat-transfer-rate distribution.

in Figs. 9 and 10. In addition, the changes in the heat-transfer-rate amplification are not due to changes in shear layer (laminar or turbulent) flow, since the shear-layer flow was turbulent. (Reynolds number was greater than the transition Reynolds number, as determined in Ref.14.) In other words, if the shock intersection point had remained constant, no change in the pressure and heat-transfer-rate distributions would have been observed. Therefore, the changes in the amplifications are due to changes in the shock intersection point, which are due to changes in the wedge boundary-layer displacement of the impinging shock. Of course, this is a Reynolds number effect.

Correlation of Peak Heat-Transfer Rates and Pressure Loads

The peak heat-transfer rates associated with types IV and III interference occur at the point at which the jet or shear layer impinges on the surface of the model. The peak heat-transfer rate for a given wedge angle or shock strength increased with the peak pressure generated by the impinging flow. This was evident, as discussed earlier, and is indicated in Figs. 9 and 10. In all cases, the peak heat-transfer rate occurred for the type IV interference pattern.

The peak heat-transfer rate depends not only on the peak pressure generated by the jet but also on the width of the jet, the angle at which the jet impinges on the surface, and whether the jet shear layers are laminar or turbulent.[4] Because the jet width and impingement angle vary with each data point, these are important factors to keep in mind during the following discussion on the heat-transfer-rate correlation. In addition, once the jet width-to-length ratio exceeds 10, the pressure decays rapidly in the jet because of mixing and increased turbulence levels.

If the jet flow is laminar and impinges nearly perpendicular to the surface, then the flow in the impingement region may be approximated by stagnation flow.[4] In order to predict the velocity gradient in the impingement region, Edney assumed that the stagnation flow in the impingement region approximated that of a two-dimensional body with a diameter equal to the jet width w. Because the process is adiabatic, there is no change in the stagnation enthalpy and, hence, the thermal driving force. Therefore, the increased heat-transfer rate in the impingement region is due to the increased velocity gradient, which is inversely propotional to the body radius and directly proportional to the stagnation pressure. Because, for laminar flow, the stagnation heat-transfer rate is proportional to the square root of the velocity gradient, the peak heat-transfer-rate amplification (q_p/q_0) can be correlated with the peak pressure amplification (p_p/p_0) by

$$q_p/q_0 = 1.41\,(r/w\,p_p/p_0)^{0.5} \tag{1}$$

Both Edney[4] and Keyes and Hains[3] reported good correlation of the experimental data with a similar relationship. The constant 1.41 in Eq. (1) is 1.03 in Edney's relationship[4] because q_0 was based on a hemisphere instead of a cylinder, as in the present investigation.

The peak heat-transfer-rate amplifications are plotted as a function of the corresponding peak pressure amplification ratio in Fig. 13. Based on the conclusion of negligible Reynolds number and small Mach number effects, the Mach 6.5 and 6.3 data are correlated together. The solid line through the origin represents the heat-transfer-rate amplification that would occur on the cylinder if it was submerged in the flow behind oblique shocks of varying strength, is represented by the pressure amplification ratio. The slope of this line on the log-log plot is 0.5, as indicated in Eq. (1). The undisturbed stagnation condition for the flow, which has been turned 10 deg, is indicated in the figure.

The type IV data (when the jet impinges on the surface as opposed to grazing or missing the surface) are seen to correlate with the square root of the pressure ratio, as indicated by the upper line. The data that falls between the two lines are from runs in which the impinging shock intersected the bow shock above the horizontal centerline, i.e., moved toward a type V interference pattern. Both sets of data show a rapid decrease in the heat-transfer-rate amplification to the level that would occur if the cylinder were completely submerged in the flow below the impinging shock (lower line).

From Eq. (1), the type IV data would correlate with the undisturbed level if $r/w = 12.5$. This would require a jet width of 0.30 cm (0.12 in.), which is equivalent to a surface arc of 11.5 deg. The schlieren measurements indicate that the jet width is 0[0.3 cm (0.1 in.)] but are not accurate enough to verify the jet width directly. Because the effect of the jet impinging on the surface is not confined solely to a region the width of the jet but is spread over several jet widths because of viscous effects of the boundary-layer interaction, the pressure and heat-transfer-rate distributions can give only a qualitative indication of the jet width. Computational fluid dynamics codes offer the best chance of verifying this simple correlation.

Similar trends are noted for the Mach 8 data presented in Fig. 14 for all three wedge angles. The data separate according to shock strength or wedge deflection angle because of the different jet widths. These data for wedge angles of 10, 12.5, and 15 deg would correlate with the undisturbed level if $r/w = 9.68$, 16.2, and 23.1 or for a jet width of 0.38, 0.24, and 0.17 cm (0.15, 0.093, and 0.065 in.), respectively. The distribution plots also indicate a narrowing of the impingement region or jet as Mach number increases.

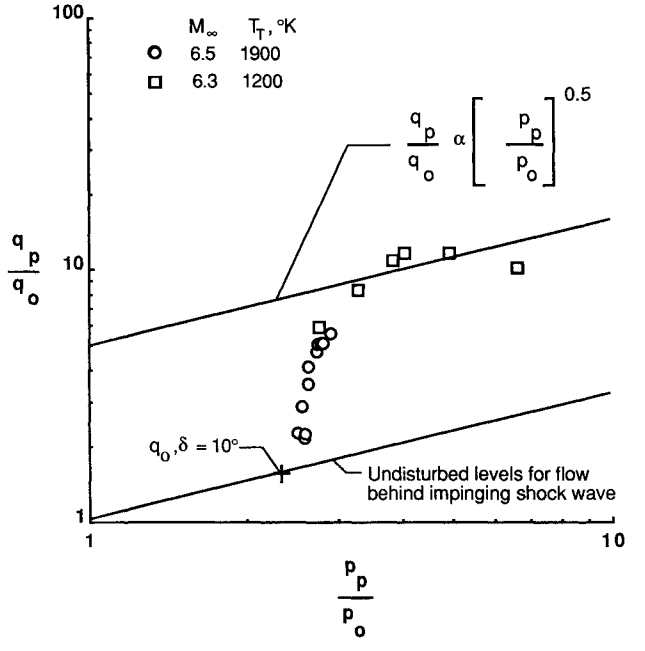

Fig. 13 Correlation of Mach 6 peak heat-transfer rate with pressure.

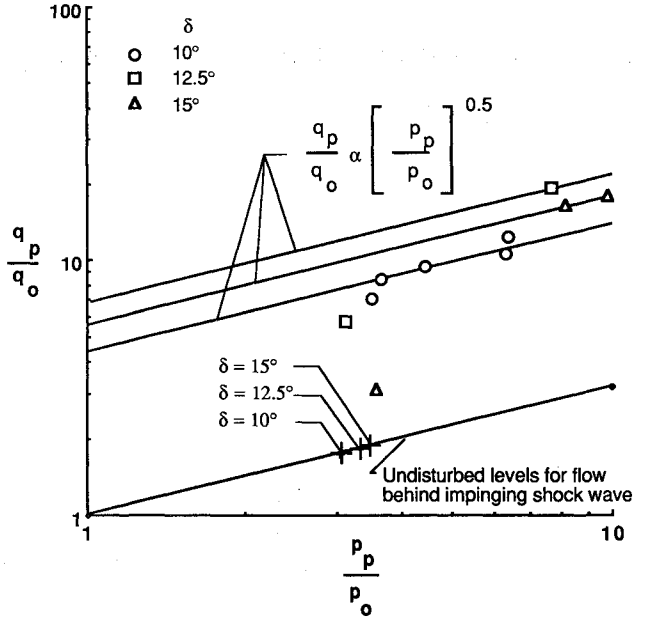

Fig. 14 Correlation of Mach 8 peak heat-transfer rate with pressure.

Concluding Remarks

This paper presents the details of an experimental study of shock-wave interference heating on a cylindrical leading edge representative of the cowl of a rectangular hypersonic engine inlet. The study was conducted at Mach numbers of 6.3, 6.5, and 8.0. Stream Reynolds numbers ranged from 1.6×10^6 to 16×10^6/cm (0.5×10^6 to 4.9×10^6/ft), and stream total temperature ranged from 1200 to 1900 K (2100 to 3400 °R). The model consisted of a 7.6-cm (3-in.)-diam cylinder and a shock generator wedge articulated to angles of 10, 12.5, and 15 deg.

The primary goal of this study was to obtain detailed surface pressure and heat-transfer-rate distributions along the circumference of the cylinder to fill a void in the data base for both design and code validation. Test results are primarily for the type IV supersonic jet interaction, since it represents the most severe pressure and heat-transfer-rate condition. However, limited results were also obtained for the type III shear-layer interaction and the type V shock interaction. The experiments were performed in the NASA Langley 8-ft High-Temperature Tunnel and the Calspan 48-in. Hypersonic Shock Tunnel, which are both capable of simulating true-temperature hypersonic flight environments.

This study has provided the first 1) detailed heat-transfer rate and pressure distributions for a two-dimensional shock-wave interference on a cylinder and 2) insight into the effects of temperature-dependent specific heats on the phenomena.

Results of the study indicate that the pressure and heat-transfer-rate distributions are asymmetric. For the type IV interaction, the heat-transfer-rate amplification (ratio heat-transfer rate caused by an interference pattern to the undisturbed flow stagnation-point level) was proportional to the square root of the pressure amplification, which is indicative of stagnation-point flow. The degree of amplification was most sensitive to the shock-wave intersection point. The peak pressure and heat-transfer-rate amplifications measured were 12.02 and 25.02, respectively, but did not occur at the same flow condition.

The amplification first increases with increasing shock strength, reaches a plateau, and then decreases with further increases in shock strength. At a given Mach number and shock strength, the amplification ratios increase as the interference pattern changes from 1) a shear layer grazing the underside of the surface to 2) a supersonic jet impinging near normally to the surface, then 3) grazing the surface as it turns to miss the surface completely by passing over the top of the cylinder.

Variation of specific heats with temperature is manifested in slightly smaller flow turning angles across shocks, which result in larger jet widths than for perfect-gas conditions. The peak pressure and heat-transfer levels, as well as the amplification ratios, were lowered as caloric imperfections increased.

References

[1]Ryan, B. M., "Summary of the Aerothermodynamic Interference Literature," Naval Weapons Center, China Lake, CA, TN 4061-160, April 1969.

[2]Korkegi, R. H., "Survey of Viscous Interactions Associated with High Mach Number Flight" *AIAA Journal,* Vol. 9, May 1971, pp. 771–784.

[3]Keyes, J. W. and Hains, F. D., "Analytical and Experimental Studies of Shock Interference Heating in Hypersonic Flow," NASA TN D-7139, May 1973.

[4]Edney, B., "Anomalous Heat Transfer and Pressure Distributions on Blunt Bodies at Hypersonic Speeds in the Presence of an Impinging Shock," Aeronautical Research Institute of Sweden, Stockholm, Sweden, FFA Rept. 115, 1968.

[5]Thornton, E. A. and Dechaumphai, P., "A Taylor Galerkin Finite Element Algorithm for Transient Nonlinear Thermal-Structural Analysis," AIAA Paper 86-0911, May 1986.

[6]Wieting, A. R., "Experimental Study of Shock Wave Interference Heating on a Cylindrical Leading Edge," Ph.D. Dissertation, Old Dominion University, Norfolk, VA, 1987; also NASA TM-100484, 1987.

[7]Craig, R. R. and Ortwerth, P. J., "Experimental Study of Shock Impingement on a Blunt Leading Edge with Application to Hypersonic Inlet Design," Air Force Applied Physics Laboratory TR-71-10, April 1971.

[8]Morris, D. K. and Keyes, J. W., "Computer Programs for Predicting Supersonic and Hypersonic Interference Flow Fields and Heating," NASA TM X-2725, May 1973.

[9]Tannehill, J. C. and Holst, T. L., "Numerical Computation of Two-Dimensional Viscous Blunt Body Flows with an Impinging Shock," *AIAA Journal,* Vol. 14, Feb. 1976, pp. 204–211.

[10]Stewart, J. R., Thareja, R. R., Wieting, A. R., and Morgan, K., "Application of Finite Element and Remeshing Technique to Shock Interference on a Cylindrical Leading Edge," AIAA Paper 88-0368, Jan. 1988.

[11]Thareja, R. R., Stewart, J. R., Hassan, O., Morgan, K., and Peraire, J., "A Point Implicit Unstructured Grid Solver for the Euler and Navier-Stokes Equations," AIAA Paper 88-0036, Jan. 1988.

[12]Carslaw, H. S., and Jaeger, J. C., *Conduction of Heat in Solids,* 2nd Ed., Clarendon Press, Oxford, England, 1959.

[13]Fay, J. A. and Riddell, F. R., "Theory of Stagnation Point Heat Transfer in Dissociated Air," *Journal of the Aeronautical Sciences,* Vol. 25, Feb. 1958.

[14]Birch, S. F. and Keyes, J. W., "Transition in Compressible Free Shear Layers," *Journal of Spacecraft,* Vol. 9, Aug. 1972.